Materials Characterization 129 (2017) 149–155

Contents lists available at ScienceDirect

Materials Characterization

journal homepage: www.elsevier.com/locate/matchar

Grain refinement and phase transition of commercial pure zirconium processed by cold rolling

Xinyi Hu, Henglv Zhao, Song Ni*, Min Song*

State Key Laboratory of Powder Metallurgy, Central South University, Changsha 410083, China

ARTICLE INFO

Keywords:
Zirconium
Grain refinement
Phase transition
Cold rolling

ABSTRACT

The grain refinement process and phase transition phenomena of a cold-rolled zirconium have been systematically investigated. The grain refinement was accomplished via a sequential series of dislocation behaviors, reaching a final grain size of < 100 nm. The refinement process can be described as: (1) dislocation nucleation, multiplication and tangling inside the original coarse-grains, (2) formation of microbands via dislocation rearrangement, (3) further division of microbands into thin laths, (4) split of microbands and thin laths into subgrains and then nanograins. Two different types of HCP-FCC phase transitions were also discovered during the cold rolling process, with the transition mechanisms and their influences on the mechanical properties being discussed.

1. Introduction

The commercial pure (CP) zirconium (Zr), a typical hexagonal close-packed (HCP) metal, has lots of promising properties, such as high tensile strength, high density, and amazing corrosion resistance. Due to these superior properties, it has attracted lots of attention for applications in various fields such as automotive, aircraft engine and biomedical materials [1–4].

Nowadays, many researchers have been focusing on the HCP structural materials, such as titanium (Ti) [5,6], magnesium (Mg) [7,8], Zr [9–14] and hafnium (Hf) [15], in order to clarify the deformation mechanisms and structure–property relationship under various deformation processes. It is known that the independent slip systems of HCP structured metals don't reach the minimum number required for homogenous deformation. Therefore, twinning is taken as a very important supplemental deformation mechanism in HCP metals [16]. In addition to dislocation slip and twinning, phase transition can also be triggered under certain stress to effectively accommodate deformation [17–19]. As for Zr, Yang et al. reported that dislocation slip is the main way for Zr to accommodate strain during cold rolling [14]. Guo et al. [9] investigated the effect of rolling strain rate on the microstructure of Zr at a temperature range of 113–183 K, and found that besides dislocation slip, twinning can also be activated to accommodate the strain and to refine the microstructure during deformation. In the present study, the microstructural evolution of Zr deformed by cold rolling was systematically investigated using transmission electron microscopy (TEM) and high-resolution TEM (HRTEM). The results indicate that dislocation slip dominated the deformation process and surprisingly, two different kinds of HCP-FCC phase transitions in Zr were also activated to accommodate the strain. The transformation mechanisms and their influences on the mechanical properties were discussed.

2. Experimental Procedure

Commercial pure Zr with a pure HCP phase was used as the raw material in this study. The chemical composition of impurities is listed in Table 1. The grains in the raw material have a mean size of 15 μm from optical microscopy analysis. Plates with a size of 30 mm × 10 mm × 5 mm (L × W × H) were rolled at room temperature with a thickness reduction of 1 mm per pass, to obtain the specimens with thickness reductions of 20%, 40%, 60% and 80%, respectively. The microstructures of un-deformed and deformed specimens were thoroughly investigated by TEM. The preparation procedure of the thin foils for TEM observation is using ion milling process: thin slices of the un-deformed and deformed specimens were cut perpendicular to the transverse direction (TD) plane with a thickness of 0.5 mm through wire-cutting, and were then mechanically thinned down to ~80 μm. Short strips with length of 3 mm were subsequently cut from the slice and were then mechanically thinned to 20 μm. By using Ganta PIPS system, these strips were ion-milled to perforation for the TEM characterization.

* Corresponding authors.
E-mail addresses: song.ni@csu.edu.cn (S. Ni), msong@csu.edu.cn (M. Song).

http://dx.doi.org/10.1016/j.matchar.2017.04.037
Received 23 March 2017; Received in revised form 30 April 2017; Accepted 30 April 2017
Available online 01 May 2017

Table 1
The chemical composition of impurities in the raw material.

Impurity elements	Sn	Nb	Fe	Cr	Cu	Hf (ppm)	C (ppm)
Content (wt%)	1.4	0.4	0.3	0.1	0.05	< 60	< 50

3. Results and Discussion

3.1. Grain Refinement

Fig. 1a shows a bright-field TEM image of the raw material. It can be seen that few dislocations and no twin can be observed inside the raw material. Fig. 1b shows a typical TEM image of the cold rolled sample with a thickness reduction of 20%. It shows that a large number of dislocations were generated, many of which tangled with each other, tending to rearrange and form dislocation walls, as indicated by red arrows in Fig. 1b. This is the very beginning of the grain refinement process.

Fig. 2a shows a TEM image of the cold rolled sample with a thickness reduction of 40%. Microband boundaries (MB boundary), originated from the former dislocation walls were observed (some examples were indicated by white arrows). These microbands have widths ranging from ~750 nm to ~4 μm. Noting that there were a high density of dislocations tangling with each other and aligning parallel to form thin lath boundaries (TL boundary) inside the microbands. Some of the lath boundaries were indicated by yellow arrows in Fig. 2b, a magnified image of the yellow rectangular region in Fig. 2a. Fig. 2c shows a bright-field TEM image of the cold rolled sample with a thickness reduction of 40% in another area, from which thin lath structure within a microband can be clearly observed and the width of the lath is < 100 nm. Meanwhile, dislocation accumulation (white arrows in Fig. 2c) can be observed within the thin laths to form dislocation walls. These dislocation walls may transversely intersect the thin laths [20].

Fig. 3a shows a bright field TEM image of the deformed specimen with a thickness reduction of 60%. It shows that the microbands formed at former strain were totally split into thin-lath structure with increasing the strain. Within the microbands these thin laths have widths ranging from several dozens of nanometers to around 300 nm. Comparing the direction of thin-lath structure in microband M1 to that in microband M2, it's apparent that the orientations of the thin-lath structure in different microbands are different. Fig. 3b shows the selected area electron diffraction (SAED) pattern of M1 and Fig. 3c shows the SAED pattern of the circled area in Fig. 3a (contains both parts of M1 and M2). Fig. 3b indicates that small misorientation exists inside the microband M1 due to the formation of thin laths. Fig. 3c indicates that large misorientation exists between two adjacent microbands M1 and M2, in which two sets of patterns with zone axes of $[11\bar{2}0]$ and $[10\bar{1}0]$ were indicated. The angle between the two zone axes $[11\bar{2}0]$ and $[10\bar{1}0]$ is around 30°, showing a high angle misorientation, while the misorientations between the thin laths are usually < 15°, which is a low angle misorientation. Fig. 3d shows another TEM image taken at a different area of the rolled specimen with a thickness reduction of 60%, where thin laths were clearly observed inside a microband. The width of these laths is generally smaller than 100 nm, indicating that the thin laths were refined longitudinally during the deformation process. Meanwhile, due to the progressive accumulation of dislocations with increasing the strain, the former transverse dislocation walls at some locations evolved into low angle or high angle boundaries. It is therefore that the areas with different contrasts can be seen in a lath, as indicated by some yellow arrows in Fig. 3d. The formation of these boundaries further cut down the thin laths into elongated subgrains and therefore transversely refined the thin laths. The (sub)grain size distribution in this stage is listed in Fig. 3e.

Fig. 4a and b shows the TEM images taken at different areas of the cold rolled specimen with a thickness reduction of 80%. In Fig. 4a, two short thin laths were indicated by dashed lines. It shows that the boundaries of these thin laths became turbulent, compared to the relatively straight ones in Fig. 3d. This configuration may be beneficial to the further transverse breakdown of the thin laths [5]. In Fig. 4b, some equiaxed grains were obviously recognizable with the average grain size of about 55 nm (see the grain size distribution diagram in Fig. 4c). An inserted SAED pattern taken from the area in Fig. 4b (upper right corner in Fig. 4b) shows diffuse arcing spots or ring shape, further confirming the formation of equiaxed nanocrystals.

The grain refinement process can therefore be concluded as following: (1) microbands formed, (2) dislocation rearranged and the formation of thin-lath structure in the microbands, (3) thin-lath structure was refined longitudinally and transversely into elongated subgrains, (4) nano-grains were formed through the further transverse refinement of the subgrains.

The dislocation slip dominated the deformation process and facilitated the grain refinement process. At the very beginning of deformation, dislocations are largely generated, as shown in Fig. 1b. They slipped on their dominant slip systems and then propagated by multiple-slip or cross-slip events [21–24]. The accumulation and tangling of these dislocations contributed to the formation of microbands. Hu et al. [25] calculated the stacking fault energy (SFE) of Zr using both local spin density approximation (LSDA) and the generalized gradient

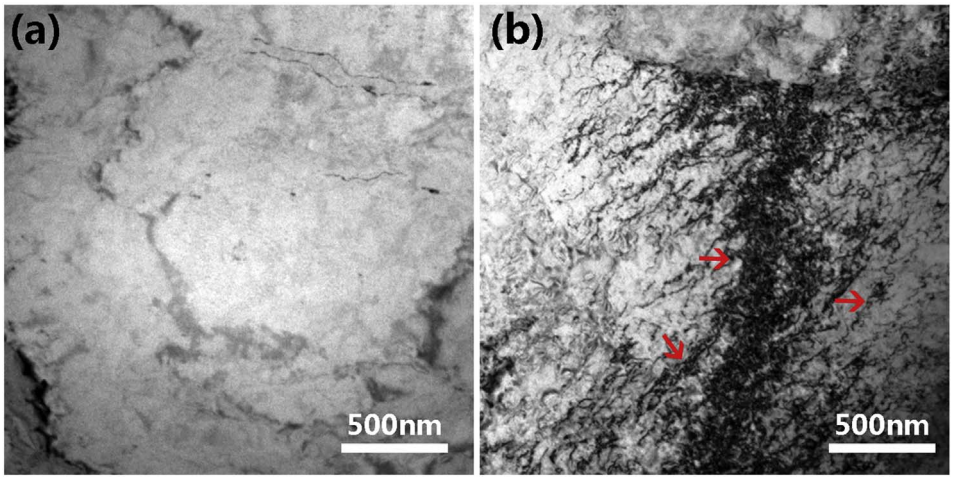

Fig. 1. TEM images of (a) the un-deformed Zr and (b) the cold rolled Zr with a thickness reduction of 20%. Note that some of the dislocation walls are indicated by red arrows. (For interpretation of the references to color in this figure legend, the reader is referred to the web version of this article.)